Hybrid Junctions of Zinc(II) and Magnesium(II) Phthalocyanine with Wide-Band-Gap Semiconductor Nano-oxides: Spectroscopic and Photoelectrochemical Characterization

Chiara Ingrosso,[†] Andrea Petrella,[†,‡] Pinalysa Cosma,[†,§] M. Lucia Curri,[§] Marinella Striccoli,[§] and Angela Agostiano*[,†,§]

Dipartimento di Chimica, Università di Bari, via Orabona 4, I-70126 Bari, Italy, CNR IPCF Sez. Bari, c/o Dipartimento di Chimica, Università di Bari, I-70126 Bari, Italy, and Dipartimento di Ingegneria Civile ed Ambientale, Politecnico di Bari, Via Orabona 4, I-70126 Bari, Italy

Received: July 26, 2006; In Final Form: September 18, 2006

The optical properties of zinc phthalocyanine ($Zn^{II}Pc$) and magnesium phthalocyanine ($Mg^{II}Pc$) in DMSO and DMF solutions have been extensively investigated, and the photoelectrochemical behaviors of layer-by-layer hybrid junctions formed of the two metallo(II) phthalocyanines ($M^{II}Pcs$) and wide-band-gap colloidal semiconductors, namely, ZnO and TiO_2 nanocrystals (NCs), have been probed. Different experimental conditions, such as the Pc center metal ion, dye concentration, and solvent identity, were investigated in order to elucidate their effects on the photoelectrochemical performances of the prepared heterojunctions. Finally, thermal treatment of either dye and NC films and control of the NC shape and surface chemistry were also studied and, interestingly, were found to be critical in affecting the performance of photochemical sensitization processes, occurring at the dye/oxide and oxide/solution interfaces.

Introduction

In the past decade, composite materials formed of thin films of organic sensitizers and inorganic nanometer-sized semiconductors have been considered appealing frameworks for energy conversion, as convenient low-cost alternative devices compared to the more expensive conventional photovoltaic cells.[1−4] Because of the fruitful combination of the peculiar properties of the two materials, such heterojunctions convert solar light into energy, mimicking the photochemical sensitization processes occurring naturally in photosynthesis.[5,6] Single-component solar cells, such as those based on bare organic semiconductors, typically present limited power conversion efficiencies, because they suffer from a low charge carrier mobility and a short exciton diffusion length (<20 nm) and because of the high energy needed to separate the photogenerated excitons.[1−3] On the other hand, nanoparticle photoactivity is restricted only to the near-UV portion of solar spectrum. The conjunction of the two materials in heterojunctions offers the possibility of overcoming these drawbacks, possibly achieving power efficiencies superior to those obtained with single-component-based photoconverter systems.[1,7,8] In hybrid junctions, the organic matrix, having a high optical density, is able to effectively harvest light, thus extending the semiconductor photoresponse into the visible spectrum. The generated excitons diffuse to the organic/inorganic interfaces, where they break up, allowing electrons to be transferred in the external circuit through the conduction band of the semiconductor. Then, the electrons reduce the solution-phase redox species at the counter (dark) electrode/solution interfaces, with the latter having already captured the localized organic oxidizing equivalents (redox species turnover).

The driving force of exciton breakup, as well as the overall cell performance, depends on the level mismatches at the inorganic/organic and organic/redox interfaces.[9,10] However, because of the complexity of the system, the cell performance also depends on many other factors: the processing conditions, the chemistry of the two constituent thin films, the coating efficiency, the pore size and distribution, the particle surface area, the electrical contact, the electrolyte composition, and the type of the interfacial redox reactions.[11−14] When nanocrystalline (NC) instead of bulk semiconductor films are used, the cell performance takes advantage of the outstanding conductivity of NCs, which ensures a unidirectional electron transport because of the continuous NC network of percolation pathways[4] and provides a relatively low rate of back electron transfer.

In addition, the peculiar properties of NCs when properly synthesized in quantum confinement regime,[6,15,16] as well as the convenient engineering of organic component provide the opportunity to tune the energy level positioning in order to define the optimal level mismatch,[17,18] thus increasing the appeal of NCs in photoelectrochemical and photovoltaic cells. The high surface-to-volume ratio of quantum-sized (Q-sized) NCs results not only in a large interfacial surface available for extensive dye coating, but also in a very efficient charge injection.[6,18] Elongated NCs can further favor interfacial charge carrier transfers because of the high density of active sites.[2]

To improve the charge injection process, the organic film should be homogeneous on the semiconductor and should be in intimate contact with it.[11] The increase in the extent of interfacial area in these hybrid systems allows for electrons to be readily injected from the lowest unoccupied molecular orbital of the dye to the conduction band of NC oxide, thus competing successfully with the exciton deactivation processes that dissipate the absorbed energy. However, significant losses of energy are further caused by exciton recombinations mediated

* Corresponding author: Prof. Angela Agostiano. Address: Dipartimento di Chimica, Università degli Studi di Bari, Via Orabona 4, I-70126 Bari, Italy. E-mail: agostiano@chimica.uniba.it. Phone: 0039-080-5442060. Fax: 0039-080-5442128.

[†] Università di Bari.

[‡] Politecnico di Bari.

[§] CNR IPCF Sez. Bari.

10.1021/jp064756h CCC: $33.50
Published on Web 11/10/2006

by trap states, resulting in incomplete percolation pathways.[19] Generally, defect states can be decreased via thermal treatment of deposited NC films.[20]

Among NC semiconductors, wide-band-gap oxides (e.g., ZnO, TiO_2) and composites (e.g., SnO_2/MgO, ZnS/ZnO, CdS/MgO, ZnO/SnO_2)[21−23] are the most promising for photoelectrochemical and photocatalysis applications, because of their photoanodic stability against degradation[24] and the low rate of direct electron−hole recombination processes.[3,25]

The high harvesting power of the organic moiety, on the other hand, should have high thermal- and photo-stability and an optical response that possibly matches the overall solar spectrum.[11] Among the available sensitizers, phthalocyanine (Pc) dyes are good candidates because of their intense Q-band in the red region of the visible spectrum and their outstanding high thermal and photochemical stability.[13,26] Phthalocyanines are the synthetic analogues of porphyrins and can be readily prepared with more than 60 different kinds of metal ions centrally ligated.[27] In addition, peripherally substituted Pcs are soluble in common organic solvents[28] and, hence, can be readily processed from solution. The possibility of modulating the spectroscopic features and tuning the electrochemical properties is thus enabled by the incorporation and modification of the metal ion at the center of the 18-π-electron aromatic macroring and/or the peripheral groups.[26,29,30] These properties make Pcs appealing materials not only for photoconversion but also for a wide range of applications as semiconductors, catalysts, optical data-storage devices,[31] photoactive materials for photodynamic therapy, photosterilization agents for blood products,[32] optical limiting substances,[27] nonlinear optical materials,[33,34] active photoreceptors in laser printing systems,[35,36] and light-emitting materials[37] and CD-R dyes.[38]

Moreover, both phthalocyanines and porphyrins represent attractive alternatives to the expensive and polluting pyridyl-based homologous (N3 dyes), offering, in addition, a higher molar extinction coefficient in the near-infrared region. However, phthalocyanine- or porphyrin-based cells still do not reach the power conversion efficiencies obtained when N3 dyes are used in the same systems (10−11%).[39] Photoelectrochemical devices based on phthalocyanine dyes are, in fact, limited by their intrinsic poor electrical conductivity,[9] because the relaxation process of excited states in Pc solid materials has been referred to exciton migration and following capture, at the radiative and nonradiative traps sites.[40,41]

Owing to the large π systems,[28] free bases and metal phthalocyanines are known to associate in the form of dimers and/or oligomers[42] through hydrogen bonds, van der Waals and electrostatic interactions, and hydrophobic effects.[43] The balance between these forces and external effects (e.g., solvent and temperature or coating process when deposited into films) determines the type of molecular assembly.[39,44,45] A large number of investigations have been focused on the aggregation behavior of Pc compounds[46−48] because these molecular assemblies have shown electrochemical, spectroscopic, photophysical, and conducting properties different from those of the corresponding monomer.[30] In the aggregates, the transition dipole moments of monomers are strongly coupled, causing changes in the absorption spectra that strongly depend on the angle (φ) between the coupled transition dipole moments and the line joining the molecule centers. If the coupling transition dipole moments are parallel to the line joining the molecular centers, in particular, if $\varphi < 54°$, "head-to-tail" or J-type aggregates result, and red-shifted transitions compared to the monomer Q-band are expected. On the contrary, if the transition dipole moments are perpendicular to the line, when $\varphi > 54°$, "head-to-head" or H-type aggregates are expected, and blue-shifted signals are detected. At present, however, only two extreme molecular assemblies have been unambiguously characterized and assigned: the molecular J-type aggregates called Jelley or Scheibe, with $\varphi = 0$, presenting extremely narrow red-shifted absorption bands, and H-type aggregates, with $\varphi = \pi/2$, characterized by blue-shifted bands.[49−55]

Some authors recently referred to aggregates having an effective role in light harvesting, because of their absorption in spectral regions wider than that of the monomer form.[56,57] Two possible routes are considered to contribute to the photocurrent generation: energy transfer to the adjacent dye molecules in monomer form, from which electrons are transferred into the conduction band of the semiconductor, or direct electron injection from the excited state of the aggregate to the nanocrystalline oxide.[58] On the contrary, most of the authors observed a reduced photosensitizing performance in the Pc aggregates, because of the quenching of the dye excited states by means of internal conversion[30] and/or because of fast energy transfers among them and the monomer excited forms,[59] using several methods to limit this tendency such as coadsorption of cheno-like hydrocarbons[60] onto NC TiO_2 electrodes or the use of additives such as 4-*tert*-butylpyridine (TBP).[61]

In this work, an extensive photoelectrochemical characterization of zinc phthalocyanine (Zn^{II}Pc) and magnesium phthalocyanine (Mg^{II}Pc)/oxide NC heterojunctions is reported. The dyes were deposited from DMSO and DMF solutions onto films of colloidal ZnO and TiO_2 NCs. The former was synthesized with either hydrolytic or nonhydrolytic methods,[62,63] the latter was synthesized with a hydrolytic approach[64] in spherical and rodlike shapes. The photoelectrochemical measurements were performed in a three-electrode photoelectrochemical cell, and $LiClO_4$ salt was tested as the supporting electrolyte. The photoelectrochemical investigation was combined with spectroscopic characterization in solution with the aim of correlating the dyes' spectroscopic properties with their photoactivity. The thermal treatments of the dyes and NC semiconductor films, the dye aggregation, the solution solvent, the semiconductor NC shape and surface chemistry, and the type of central metal ion were investigated to obtain information on the photoelectrochemical performance of the prepared heterojunctions.

Experimental Methods

Materials. All chemicals were of the highest purity available and were used as received without further purification. Zinc phthalocyanine (Zn^{II}Pc), magnesium phthalocyanine (Mg^{II}Pc), dimethylformamide (DMF), and dimethyl sulfoxide (DMSO) were purchased from Avocado Research Chemicals Ltd., Merck, and Sigma Aldrich, respectively.

Zinc acetate dihydrate ($C_4H_6O_4Zn{\cdot}2H_2O$ or $ZnAc_2{\cdot}H_2O$), anhydrous zinc acetate ($ZnAc_2{\cdot}H_2O$), *tert*-butylphosphonic acid (TBPA), titanium tetraisopropoxide [$Ti(O^iPr)_4$ or TTIP, 99.999%], trimethylamino-*N*-oxide dihydrate [$(CH_3)_3NO{\cdot}2H_2O$ or TMAO, 98%, water solution], anhydrous ethylene glycol [$HO(CH_2)_2OH$ or EG 99.8%], oleid acid ($C_{18}H_{33}CO_2H$ or OLEA, 90%), analytical-grade chloroform ($CHCl_3$), ethanol (C_2H_5OH), and methanol (CH_3OH) were purchased from Aldrich. Hexadecylamine (HDA), dodecylamine (DDA), tri-*n*-octylamine (TOA), $LiOH{\cdot}H_2O$, and $LiClO_4$ were purchased from Fluka Biochemika. All aqueous solutions were made using bidistilled water. Indium tin oxide (ITO) substrates were supplied by Merck.

Synthesis of ZnO NCs. ZnO nanocrystals were synthesized using two different preparative approaches.

Nonhydrolytic Synthesis of ZnO NCs. Nearly spherical nanosized organic-capped colloidal ZnO NCs ($d < 10$ nm) were prepared by a nonhydrolytic approach.[62] $ZnAc_2$ was thermally decomposed at 220−300 °C in long-chain alkylamines (HDA, DDA, or TOA) and in the presence of the size-regulating agent TBPA. It was demonstrated that the parameter that effectively modulates the nanoparticle mean size is the precursor/regulant agent molar ratio ($R = ZnAc_2$/TBPA), which was adjusted to a value of $R = 0.15$, to obtain a final mean particle size of about 6 nm. The as-prepared NCs were precipitated by the direct addition of an excess of methanol in the reaction mixture. After repeated washing with ethanol to remove excess TBPA and residual chemicals, the TBPA-capped NCs were dissolved in $CHCl_3$, resulting in optically clear solutions.

Hydrolytic Synthesis of ZnO NCs. Quantum-confined nearly spherical ZnO colloidal NCs (6 nm in size) were prepared by a hydrolytic approach.[63] A 0.1 M ethanol solution of $ZnAc_2 \cdot H_2O$ was used in which Zn acts as the precursor. The addition of $LiOH \cdot H_2O$ powder has been demonstrated to accelerate the release of OH ions, resulting in an immediate reaction to form a stable ZnO nanoparticle solution.

Synthesis of TiO_2 NCs. Organic-capped anatase TiO_2 NCs were synthesized by the hydrolysis of the precursor titanium tetraisopropoxide (TTIP) using technical oleic acid (OLEA) as the surfactant at low temperature (80−100 °C), as reported elsewhere.[64] The precursor hydrolysis was carried out with an excess of aqueous base TMAO solution, which catalyzes the polycondensation. The particle size and aspect ratio were changed by varying the TTIP concentration in the growing mixture and/or the reaction time. Nearly spherical or rod-shaped NCs were obtained by varying the rate of water supply in the reaction flask. Nanorods (30 nm in length and 3−4 nm in diameter) were obtained by direct injection of large aqueous TMAO volumes into OLEA/TTIP mixtures, whereas nearly spherical particles (6 nm in size) were obtained upon the slow in situ release of water resulting from the esterification of OLEA and EG.

After precipitation and washing with methanol, the OLEA-capped TiO_2 NCs were dispersed in optically clear $CHCl_3$ solutions.

Layer-by-Layer Hybrid Junction Setup. Chloroform solutions (0.1 M) of ZnO and TiO_2 NCs were deposited by either casting or spin-coating onto optically transparent electrodes of indium tin oxide (ITO). The NC films were thermally treated at 150 or 350 °C for ∼30 min to facilitate oxide adhesion onto the ITO surface, to completely remove the solvent or contaminants, and to ensure a continuous film for charge percolation. $Zn^{II}Pc$ and $Mg^{II}Pc$ were deposited from 10^{-3} M DMF and DMSO solutions onto the semiconductor films and then were heated at 350 °C for ∼10 min to guarantee complete solvent removal and to allow for better dye adsorption on the nanocrystalline surface.

Characterization of Samples. *UV−Vis, Photoluminescence, and Resonance Light-Scattering Spectroscopies.* UV−vis absorption, reflectance, photoluminescence (PL), and resonance light-scattering (RLS) measurements were made at room temperature. UV−vis absorption and reflectance spectra were recorded using a Cary 5 (Varian) UV−vis−NIR spectrophotometer, whereas PL and RLS spectra were recorded with a Varian Cary Eclipse spectrofluorimeter.

PL measurements were performed on 10^{-7} M dye solutions after a 30-min degassing step with N_2 for $Zn^{II}Pc$ and with Ar for $Mg^{II}Pc$. The chosen excitation wavelengths were 320 and 600 nm, and a 25% transmittance filter was used for the RLS spectra.

Powder X-ray Diffraction. XRD patterns of ZnO and TiO_2 NC powders were collected with a Philips PW 1729 diffractometer in a conventional $\theta-2\theta$ reflection geometry using filtered Cu Kα radiation ($\lambda = 1.54056$ Å). The ZnO and TiO_2 nanocrystalline powders were placed on aluminum and silicon sample holders, respectively.

Transmission Electron Microscopy. Transmission electron microscopy (TEM) images of ZnO and TiO_2 NC samples were obtained using a Philips CM-300 UT microscope (TEM) operating at 300 kV. The ZnO and TiO_2 samples were prepared by dropping dilute solutions of isolated nanoparticles in chloroform onto 400-mesh carbon-coated copper grids and immediately evaporating the solvent. The samples were stable under the electron beam and did not degrade within the typical observation time.

Photoelectrochemical Measurements. The photoelectrochemical investigations were conducted at room temperature in a three-electrode cell using an Autolab PGSTAT 10 potentiostat. In this system, Ag/AgCl (3 M KCl, $E° = 0.241$ V vs SHE) is the reference electrode, a platinum wire is the counter electrode, ITO is the working electrode, and 0.1 M bidistilled water solutions of $LiClO_4$ salt were used as the supporting electrolyte. During photoelectrochemical measurements, a constant bias of 0 V was imposed between the reference and counter electrodes. The heterojunctions were illuminated with an optical-fiber tungsten lamp (250 W).

Results and Discussion

Chloroform solutions of nonhydrolytically prepared ZnO NCs and hydrolytically prepared nearly spherical TiO_2 NCs exhibit the UV−vis absorption spectra reported in Figure 1. The hydrolytically prepared ZnO and elongated titania NCs (data not shown) exhibit similar spectroscopic and morphological characteristics. All of the nanocrystalline oxides show absorption onsets that are blue-shifted with respect to that of the corresponding bulk semiconductor.[62−64] The X-ray diffraction patterns match the wurtzite and anatase profiles for ZnO and TiO_2 nanopowders, respectively (see Figure 1). The broadening of the diffraction peaks for both nano-oxides points out the occurrence of nanosized crystalline domains and allows for the estimation of the main nanocrystal size, which results in good agreement with the value measured by TEM (see Figure 1).

In Figures 2 and 3 are reported the absorption and emission spectra, respectively, of the D_{4h}-symmetric $Zn^{II}Pc$ and $Mg^{II}Pc$ dyes, whose molecular structures, presenting 18 π electrons delocalized on the Pc ligand, are reported in Chart 1. The metal phthalocyanines were dissolved in DMSO, which is reported to limit the aggregation of Pc dyes,[65] and in another solvent of similar polarity, namely, DMF. In the visible part of the spectra, the signals attributed to $\pi-\pi^*$ transitions among S_0-S_1[66] states, according to Gouterman's four-orbital LCAO model, are evident. The Q_{0-0} bands of monomer $Zn^{II}Pc$ in both solvents are located in the 650−700-nm range (see Figure 2), in agreement with data reported in the literature.[26] These strong, narrow features, are well-known to be sensitive to the Pc symmetry, the presence and position of peripheral moieties, the presence of the central metal ion, the type of metal, and the Pc environment.[30,67] Going to the blue side, the peak attributed to dimers or higher-order H-type aggregates (625−650 nm),[43,49−54,68] originating from dipole−dipole interactions,[66] and the monomer Q_{0-1} vibronic peak[69] (580−625 nm) can be observed. The broad absorption signals in the near-UV region (300−400 nm) are

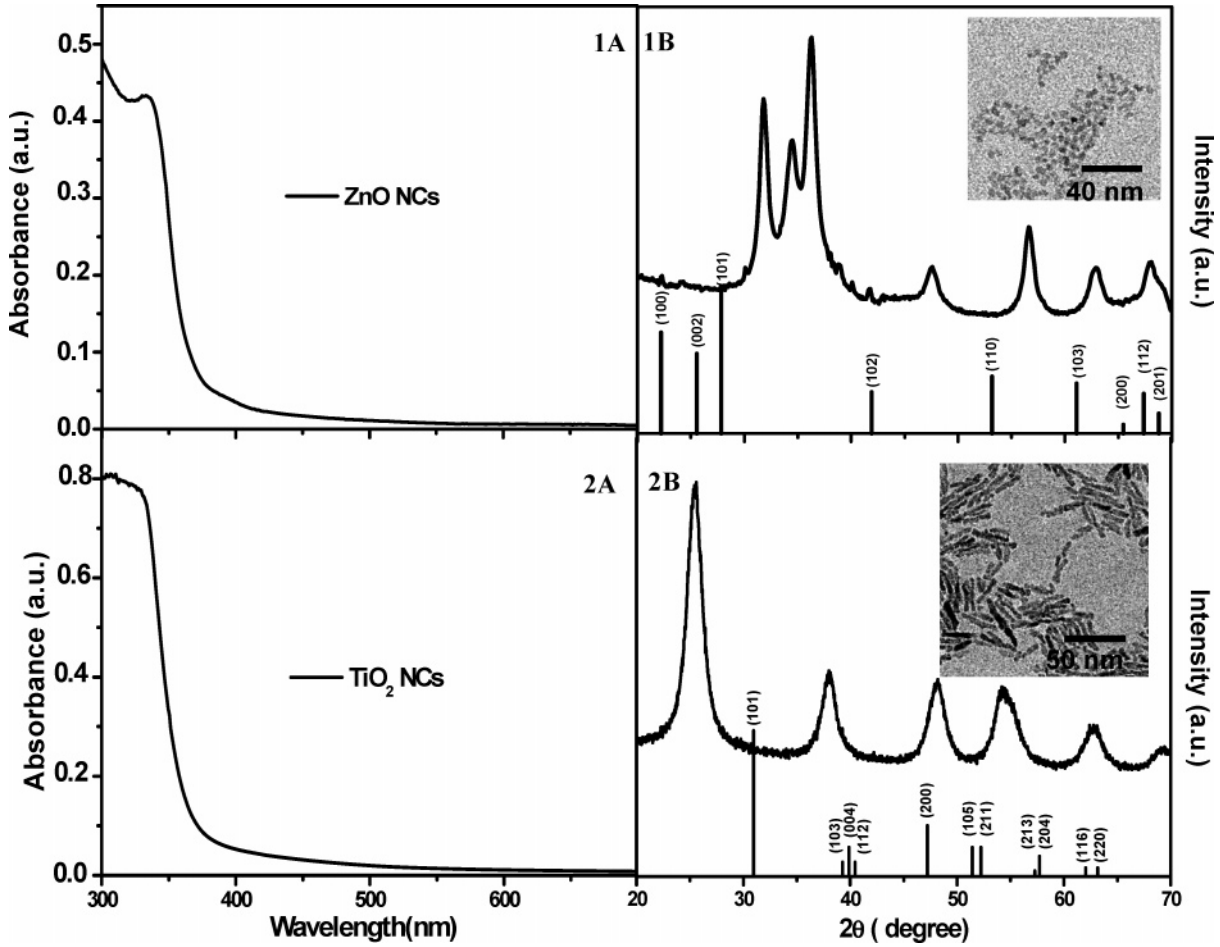

Figure 1. UV−vis absorption spectra of 10^{-3} M chloroform solutions of (1A) nearly spherical nonhydrolytically prepared ZnO NCs and (2A) nearly spherical hydrolytically synthesized TiO_2 NCs. X-ray diffraction patterns of (1B) ZnO and (2B) TiO_2 nanoparticle powders compared to the wurtzite ZnO and anatase TiO_2 diffraction profiles. Insets: TEM overviews of (1B) as-prepared ZnO NCs with $R = 0.15$ and (2B) TiO_2 NCs.

instead attributable to the Soret band (B_1,B_2 transitions). Increasing the dye concentration does not result in any significant modification of the absorption spectrum profile (Figure 2)

The absorption spectra of Figure 2, for $Mg^{II}Pc$ in DMSO and DMF, exhibit quite different behavior, as a stronger tendency of the dye to aggregate is evidenced in both solvents. In DMSO, the signal located at 630 nm can again be attributed to H-type aggregates,[43,49−54] and an increase of the concentration results in the rise of a peak on the red side, centered at 717 nm, ascribable to J-type molecular assemblies. The monomer peak remains confined to 674 nm in both solvents. In DMF, the growth of the H- and J-type aggregate bands, located at 615 and 709 nm, respectively, with increasing the dye concentration is also more marked.[43,49−54]

The different spectroscopic behaviors of the two investigated $M^{II}Pc$ dyes are related to the different electronegativities, electronic configurations, and dimensions of the central metal ion,[26,30] which determine the energies and degeneracies of the molecular orbitals.[70] $Zn^{II}Pc$ and $Mg^{II}Pc$ are both considered planar structures with D_{4h} symmetry, as demonstrated by ab initio Hartree−Fock structural optimization of $M^{II}Pc$ molecules.[71,72] Magnesium is an alkaline-earth metal with empty 3d orbitals that can be easily employed in coordination. The tetracoordinate Mg ion can, therefore, further coordinate molecules to form aggregates. In fact, the Mg ion is most stable in its octahedral coordination, as largely evidenced by studies on chlorophyll aggregation in organic solvents.[73] The Zn ion, conversely, generally utilizes the $4s_0$ and $4p_0$ orbitals to coordinate four ligands in a tetrahedral structure, and therefore, it tends to remain tetracoordinated.

In $Mg^{II}Pc$, the lack of electrons in the Mg d orbitals results in molecular electronic transitions originating basically from the Pc ligand,[74] reducing the π-electron delocalization and simultaneously decreasing the molar extinction coefficient of the molecule; in fact, $Zn^{II}Pc$ shows an higher molar extinction coefficient in both solvents. The absence of fully occupied d orbitals is also responsible for the reported nonplanar configuration of the $Mg^{II}Pc$ single crystal, in which the central atom is statistically distributed over the top and bottom of the molecule symmetry center,[75] and for the formation of J-type aggregates observed for this phthalocyanine.

The interactions between the dye and the solvent modify the electronic density of the Pc molecules, resulting in changes in the absorption spectrum,[68] as evidenced by the behavior of the dyes reported in Figure 2. For $Zn^{II}Pc$, the differences are limited to only a higher molar extinction coefficient and a red shift of the monomer Q_{0-0} bands in DMSO. The increase of the refractive index on going from DMF to DMSO and the specific σ-donating coordination of DMSO to the nitrogen bridges of the Pc macrocycle (soft oxidizing effect), which stabilizes the S_1 excited state,[76] can reasonably account for both pieces of experimental evidence. A more surprising effect is then exerted by DMF on $Mg^{II}Pc$, where the formation of H-type aggregates is strongly promoted compared to equally concentrated dye solutions in DMSO. The two solvents are both considered weakly coordinating agents[76,77] and have quite similar solvent parameters (see Table 1).

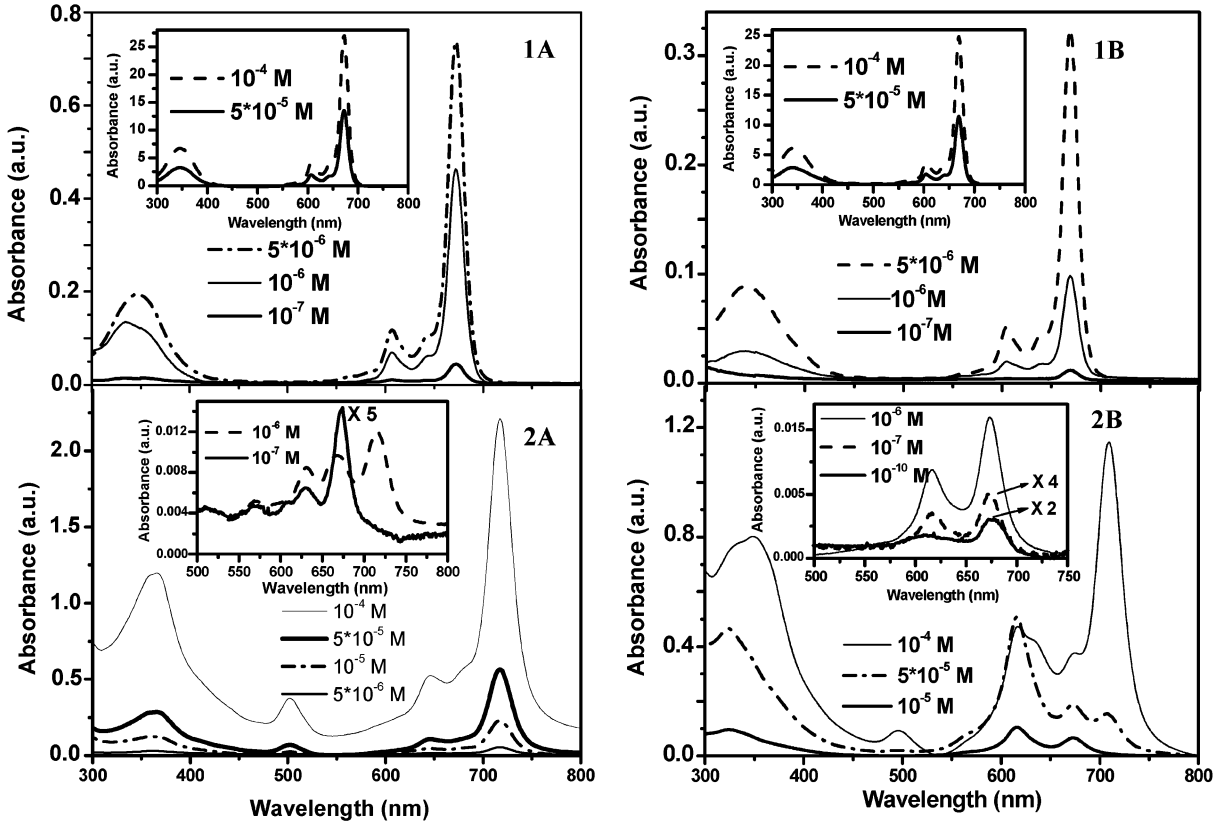

Figure 2. UV−vis absorption spectra of $Zn^{II}Pc$ (1A, DMSO; 1B, DMF) and $Mg^{II}Pc$ (2A, DMSO; 2B, DMF) with increasing concentration. Insets: absorption spectra of concentrated $Zn^{II}Pc$ in (1A) DMSO and (1B) DMF solutions and of dilute $Mg^{II}Pc$ in (2A) DMSO and (2B) DMF solutions. The traces corresponding to the 10^{-7} and 10^{-10} M $Mg^{II}Pc$ solutions in the insets of 2A and B were magnified by the factors indicated.

The more significant difference resides in the value of the dielectric constant, notably lower in DMF, that, therefore, seems to play a role in the formation of Pc head-to-head-type aggregates.

In Figure 3, the photoluminescence emission intensities of 10^{-7} M $Zn^{II}Pc$ and $Mg^{II}Pc$ in DMF and DMSO recorded after excitation at 600 nm are reported. The PL spectra present signals located in the 650−700-nm range, attributable to monomer emission. The form and position of the monomer band are independent of the excitation wavelength, as evidenced in Figure 3C and D.

As can be seen, $Zn^{II}Pc$ presents a significant higher emission intensity in DMSO than in DMF, whereas $Mg^{II}Pc$ generally shows a low emission that increases in DMF. Furthermore, the almost-negligible Stoke's shifts (see insets of Figure 3A and B) observed for both dyes in the two solvents indicate a rather low tendency to relax through energy transfers with the neighboring dye molecules or through other nonradiative deactivation pathways, because of the intrinsic dye molecular rigidity.[26]

Comparison of the PL scales of Figure 3A and B indicates that $Zn^{II}Pc$ presents a significantly higher emission intensity than $Mg^{II}Pc$, irrespective of the solvent. This result can again be related to the presence of empty d orbitals, which provides cascade relaxations between the highest occupied molecular orbitals (HOMOs) and the lowest unoccupied molecular orbitals (LUMOs) of the Pc ligands, mediated by the internal levels of the metal ions[78] or through ISC to the triplet states of the Pc ligands.[78,79] In addition, the low emission of $Mg^{II}Pc$ can also be ascribed to the large presence of aggregates.

The strong tendency of $Mg^{II}Pc$ to aggregate is further supported by the resonance light-scattering data reported in Figure 4. This technique is strongly advised for the detection of chromophore aggregation.[80,81]

The RLS phenomenon arises from an enhancement of the scattered light intensity in the red edge portion of an absorption band and allows for the specific identification of aggregated chromophores, even in complex matrixes. The conditions to be met for observing this effect are a strong electronic coupling between adjacent chromophores, a large size and proper geometry of the resulting aggregate, and an intense molar absorbance of the monomer unit.

The RLS signal in the 400−500-nm region, which increases with increasing concentration (spectra not reported), can be definitively assigned to the presence of aggregates. Two considerations, based on the absorption data in Figure 2, seem to suggest the H-type nature of these aggregates: the fact that this signal is present in the spectra of both $M^{II}Pcs$ and the stronger intensity of the scattering for $Mg^{II}Pc$, reflected by the intense absorption band for this type of molecular assembly (see Figure 2), when recorded at the same dye concentration.

The RLS signals around 600 nm and those at wavelengths greater than 700 nm are, conversely, present only in the spectrum of $Mg^{II}Pc$ and can reasonably be attributed to the presence of J-type aggregates of different sizes. The observed band at around 700 nm in the two samples of $Zn^{II}Pc$ with different concentrations is due to the PL emission of the dye (see Figure 3). The weak red shift of this emission band is attributable to the dye self-absorption effect.

The tendency of MPcs to aggregate is, as expected, higher when the dyes are deposited onto films. In Figure 5 are reported the reflectance spectra of $Zn^{II}Pc$ and $Mg^{II}Pc$ hybrid junctions on nonhydrolytic ZnO NC films deposited onto ITO. In the red part of the spectrum, the Mg-based dye exhibits the same peaks

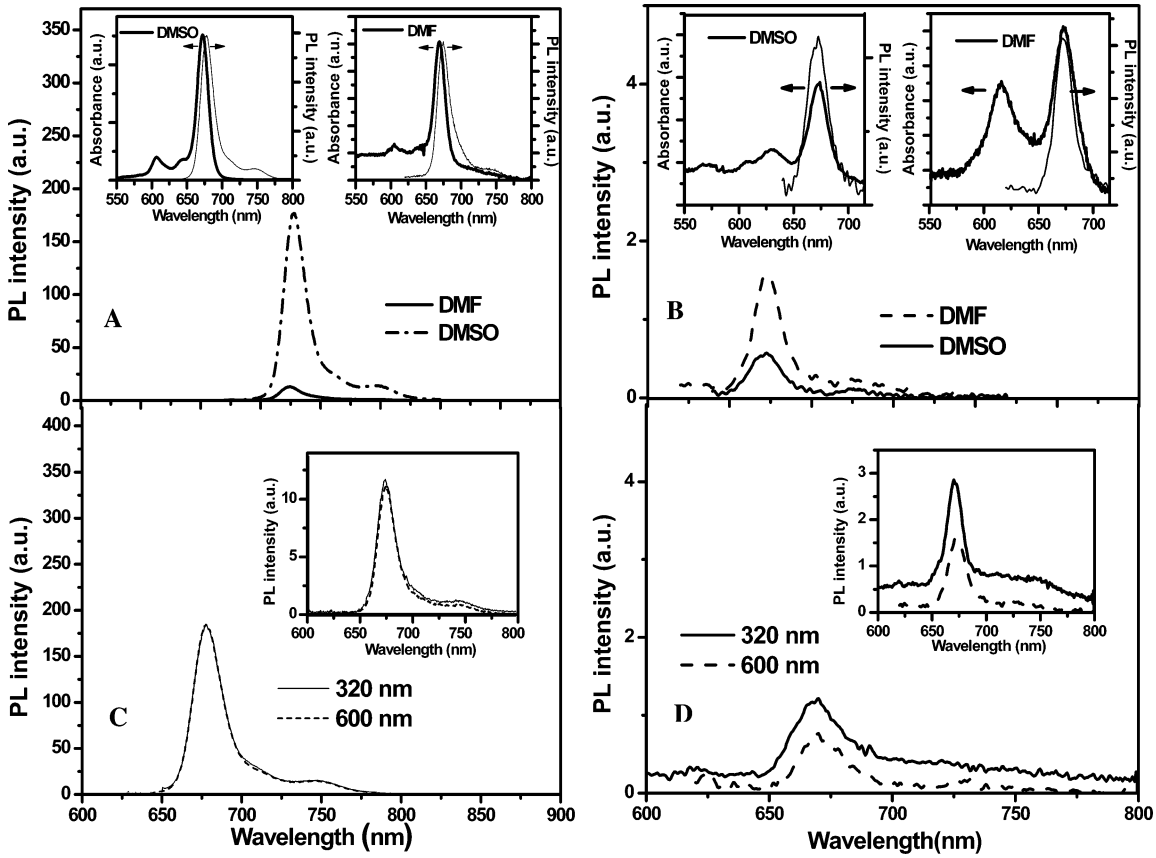

Figure 3. Photoluminescence emission spectra of 10^{-7} M (A) $Zn^{II}Pc$ and (B) $Mg^{II}Pc$ in DMSO and DMF solvents, at the excitation wavelength of $\lambda = 600$ nm. Insets: Stoke's shift of (A) 10^{-7} M $Zn^{II}Pc$ in DMSO (top left) and DMF (top right) and (B) 10^{-7} M $Mg^{II}Pc$ in DMSO (top left) and DMF (top right). Photoluminescence emission spectra of 10^{-7} M (C) $Zn^{II}Pc$ and (D) $Mg^{II}Pc$ in DMSO solvent, at excitation wavelengths of 320 and 600 nm. Insets: Photoluminenscence of 10^{-7} M $Zn^{II}Pc$ and $Mg^{II}Pc$ DMF solutions, at excitation wavelengths of 320 and 600 nm. The spectra were recorded after 30 min degassing with N_2 for $Zn^{II}Pc$ and with Ar for $Mg^{II}Pc$.

CHART 1. Molecular Structures of $Zn^{II}Pc$ and $Mg^{II}Pc$

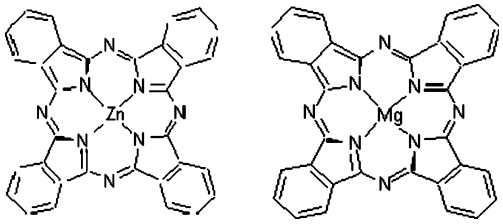

TABLE 1. Solvent Parameters

solvent	ϵ_r	μ/Δ	DN[a]	AN[a]
DMF	36.71	12.9	26.6	16
DMSO	46.45	13.0	29.8	19.3

[a] DN, donor number; AN, acceptor number.

as shown in Figure 2, although broader, attributed to the monomer and to H- and J-type aggregates. More surprising is the spectrum of $Zn^{II}Pc$, whose profile is quite different from that recorded in solution, exhibiting bands at wavelengths greater that 750 nm, characteristic of highly aggregated polymeric species, possibly originating through interactions with the nanostructured ZnO film. Moreover, the presence of these aggregates is also evidenced by the steep increase of the scattering signal in the far red region of the RLS spectrum observed for a highly concentrated dye solution, reported in the inset of Figure 5, thus suggesting that a concentration effect could more likely be invoked, rather than dye interactions with the oxide support.

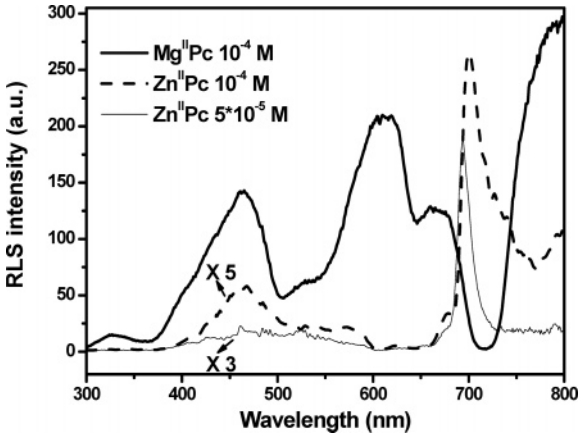

Figure 4. RLS spectra of 10^{-4} M $Mg^{II}Pc$ and 10^{-4} and 5×10^{-5} M $Zn^{II}Pc$ DMSO solutions. The traces corresponding to the 5×10^{-5} and 10^{-4} M $Zn^{II}Pc$ solutions were magnified by the factors indicated.

Films of the $M^{II}Pcs$ deposited onto ZnO nano-oxide were photoelectrochemically characterized, and the results are reported in Figure 6 and compared to the data obtained from bare $M^{II}Pcs$ and ZnO NC films.

The analysis of the light-generated currents in a photoelectrochemical cell is always a complex problem, because of the concurrent contribution of charge transport inside the film and charge injection toward the electrodes and/or electrolyte solution. Consequently, the NC surface chemistry and shape, the morphology of the films in contact with the solution, and the solution composition play significant roles.

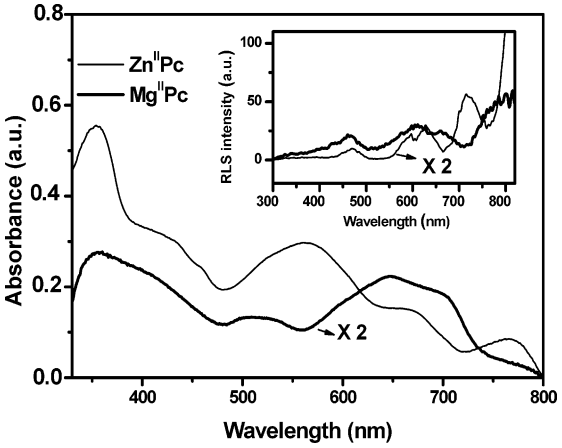

Figure 5. Absorption spectra in reflectance mode of 5×10^{-3} M Zn^{II}Pc and Mg^{II}Pc DMSO solutions cast onto ZnO NC films (nonhydrolytically prepared). The NC film was cast onto an ITO-coated substrate from a 0.1 M $CHCl_3$ solution and treated at 350 °C, and the dye films were placed under vacuum at room temperature. Inset: RLS spectra of 5×10^{-2} M Zn^{II}Pc and Mg^{II}Pc DMSO solutions. The absorption spectrum of Mg^{II}Pc and the RLS signal of Zn^{II}Pc were magnified by the factors indicated.

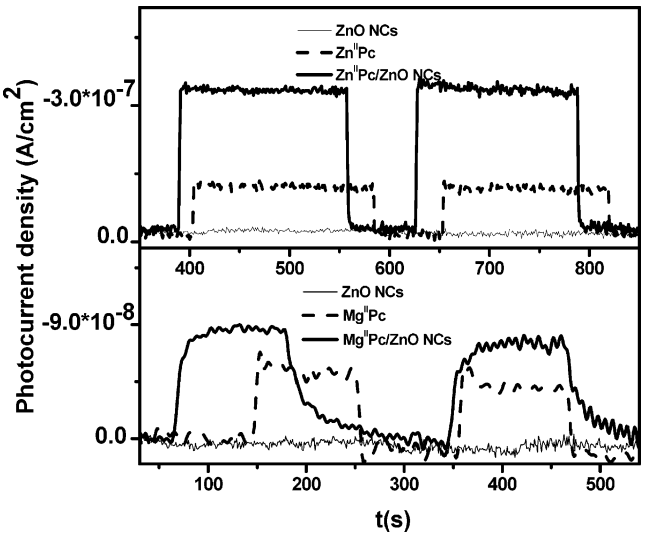

Figure 6. Photoelectrochemical measurements of (top) Zn^{II}Pc- and (bottom) Mg^{II}Pc-sensitized ZnO NC films (hydrolytically prepared) compared to the response of bare dye electrodes and bare ZnO NC-based films. The cast ZnO NC films were treated at 150 °C, and the cast dyes were treated at 350 °C.

The recorded increase in the photocurrent signals for the heterojunctions, compared to those of the single components, demonstrates that both dyes behave effectively as light harvesters, performing electron injection processes in ITO and oxide NC conduction bands, and that a relatively effective matching is established between the dye LUMO and the NC oxide conduction band.

The improvement of the photoactivity is also due to the overcoming of the intrinsic low charge mobility typical of organic layers[1] through the outstanding conductivity of inorganic nanocrystalline semiconductors.[4] Additionally, the presence of the NC film is expected to thermodynamically favor electron transfer from the dye to the ITO.[14,82]

The experimental evidence of detectable photocurrents for bare dye electrodes supports the establishing of a potential p−n junction, thus confirming the p-type semiconducting behavior of Zn^{II}Pc and Mg^{II}Pc, ascribed to the extensive π-conjugated system of the 18 mobile π electrons.[39,83] In addition, oxygen

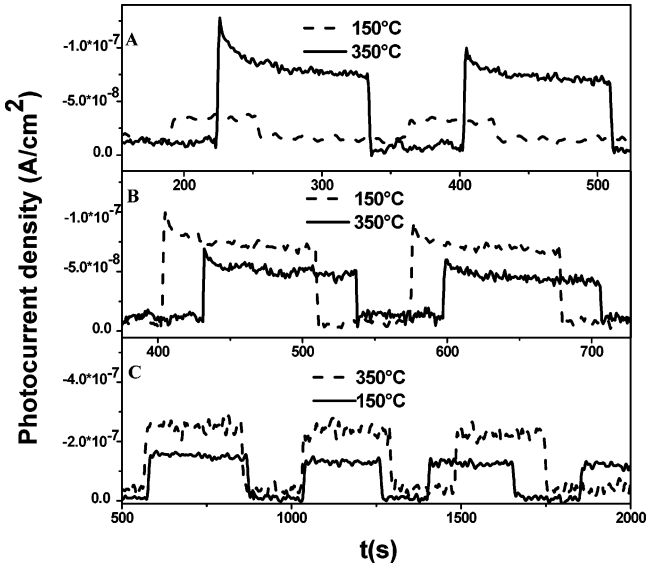

Figure 7. Photocurrents of Zn^{II}Pc-sensitized hydrolytically or nonhydrolytically prepared ZnO NC electrodes. (A) Hydrolytic ZnO NC films treated at 150 °C and then Zn^{II}Pc treated at 150 and 350 °C. (B) Hydrolytic ZnO NC films treated at 150 and 350 °C and Zn^{II}Pc treated at 350 °C. (C) Nonhydrolytic ZnO NC films treated at 150 and 350 °C and Zn^{II}Pc treated at 350 °C. The NC and Zn^{II}Pc films were deposited by spin-coating, and the dye was spin-coated from DMSO solution.

molecules strongly bound to MPcs have been suggested to act as dye p-dopants,[84] resulting in the formation of a space layer at the ITO/dye interface, and dye p-doping has been demonstrated to occur also with oxygen that originates from the ITO surface.[85]

The thermal treatment was found to play a significant role in the photoelectrochemical response of the electrodes, as evidenced in Figure 7, where the performances obtained from bare Zn^{II}Pc films and hydrolytic and nonhydrolytic ZnO NC-based films, treated at different temperatures, are reported. The results for the dye treated at 150 and 350 °C (Figure 7A) after deposition onto hydrolytic ZnO indicate a strong improvement of the photocurrents with increasing temperature. Identical results were obtained with nonhydrolytic ZnO NCs. The high photoactivity observed at 350 °C could reasonably be related to the permanent Zn^{II}Pc phase change, from the α form to the more conductive β form, occurring above 300 °C.[86]

Regarding the different preparation routes for the nanocrystals, the best photoelectrochemical performances were obtained after treatment at 150 and 350 °C, respectively, for the hydrolytic and nonhydrolytic ZnO NC films (see Figure 7B and C). For the former, the decreased photoactivity at the highest temperatures can be ascribed to a phase change of the acetate groups originating from the synthesis precursor bound to the NC surface.[63] At about 180 °C, these groups start changing from the unidentate to the bidentate form, which is able to capture the electrons during the interfacial charge separation processes.[87] Furthermore, the negatively charged acetate groups in the unidentate form repulse the injected electrons, resulting in the highest photocurrent observed at 150 °C. Conversely, the highest photocurrents after treatment at 350 °C recorded for the heterojunctions based on nonhydrolytic ZnO NCs can likely be attributed to the quantitative removal of the insulating TBPA organic capping ligand[2,13,14] achieved at that temperature.

As can be observed in Figure 7, the photocurrents recorded for the hydrolytic ZnO NC films are generally lower than those of the nonhydrolytic homologues. This result can be related to the presence of −OH groups on the surface of the nano-oxide,

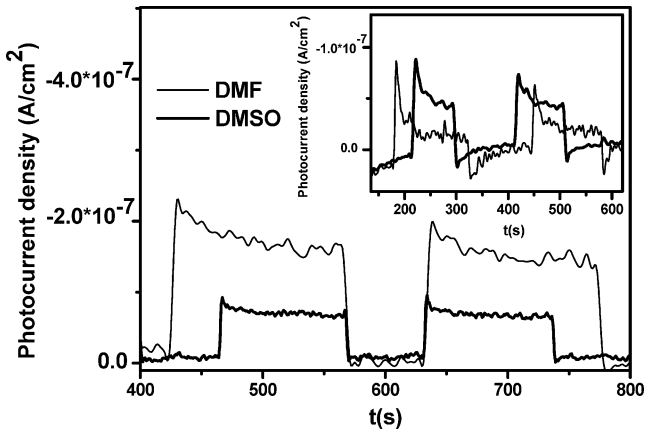

Figure 8. Comparison of the photoelectochemical responces of $Zn^{II}Pc$- and (inset) $Mg^{II}Pc$-sensitized ZnO NC films (hydrolytically prepared) spin-coated from DMSO and DMF solutions at the same concentration. The spin-coated ZnO NC films were treated at 150 °C, and the spin-coated dyes were treated at 350 °C.

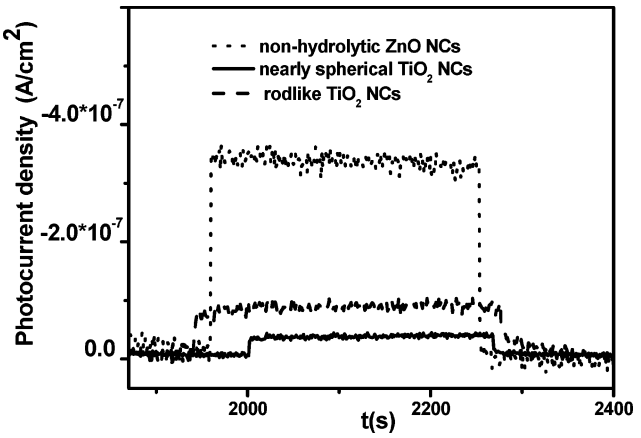

Figure 9. Photocurrents of $Zn^{II}Pc$-sensitized nonhydrolytic ZnO and spherical and rodlike TiO_2 NC hybrid junctions. The spin-coated dye was deposited from DMF solutions onto NC films, and both components were treated at 350 °C.

acting as surface trap states, although the role of the insulating lithium ion shells that surround the hydrolytically prepared ZnO nanoparticles cannot be ruled out. The nature of the solvent from which both $Zn^{II}Pc$ and $Mg^{II}Pc$ were deposited onto the nanocrystalline electrodes, determining the aggregation processes in solution, influences the photocurrent behavior, as reported in Figure 8. Particularly significant is the strong decrease observed for $Mg^{II}Pc$ in DMF compared to $Zn^{II}Pc$, which, according to the absorption data in Figure 2, can reasonably be attributed to the formation of H-type aggregates. For both dyes, an effect of quenching of the photocurrents with increasing dye concentration is also evident (data not shown). These results, according to the absorption data in Figure 2, further highlight the detrimental effect of the dye aggregates, because they do not participate in charge injection processes, quenching the dye excitons by internal conversion[30] and/or by fast energy transfers with the monomer excited forms.[59] The higher photocurrents recorded for $Zn^{II}Pc$ deposited from DMF can also be correlated with the photoluminescence properties of the dye, reported in Figure 3. The insets of Figure 3 for $Zn^{II}Pc$ point out that the thermal deactivation of excited $Zn^{II}Pc$ is almost negligible, and previously reported data support the weak contribution of the slow thermal triplet-state relaxation.[26] As a consequence, only the fluorescence decay can effectively compete with the dissociation of $Zn^{II}Pc$ excitons. The lower dye fluorescence in DMF compared to that observed in DMSO could consequently explain the higher tendency of $Zn^{II}Pc$ excitons to dissociate, resulting in higher photocurrents.

Finally, the role played by the nature and shape of the nanocrystal in the sensitization effect of $M^{II}Pcs$ was studied by comparing the photocurrents of nonhydrolytic ZnO-based heterojunctions with those obtained for spherical and rod-like hydrolytic TiO_2 NC films (see Figure 9). The oxide NC films were treated under the same experimental conditions: sensitized with 10^{-3} M $Zn^{II}Pc$ and thermally treated at 350 °C. The observed decrease in the photoactivity of the TiO_2 NCs can be attributed to the insulating layer of the OLEA capping, which coordinates the surface of the hydrolytically prepared nanocrystals.[2] A slight increase of the photocurrent intensity was observed for rodlike TiO_2-NC-based hybrid junctions with respect to those formed by nearly spherical nano-oxides. Elongated NCs are expected to bring considerable advantages in photosensitizing processes compared to spherical nanoparticles, because they can be packed in a more efficient configuration because of the larger contact area and the stronger van der Waals interactions.[2,88] In addition, the increased carrier delocalization in such shaped NCs also reduces the e^-/h^+ recombination probability. The lower enhancement of the photocurrents for rodlike TiO_2 NCs suggests a random orientation of the elongated NCs in the hybrid junctions,[89] which consequently reduces charge diffusion processes and charge transport along the film, thus limiting the number of percolation pathways available for the injection of electrons.[3]

In conclusion, the different electronic configurations of the central metal ion of the two dyes result in different spectroscopic and photoelectrochemical properties. Although $Zn^{II}Pc$ and $Mg^{II}Pc$ dyes are indicated to exhibit the same photoelectric behaviors in the literature,[26] our data seem to point to a lower photoactivity of $Mg^{II}Pc$ compared to $Zn^{II}Pc$ when deposited on ZnO NC films. The thermal treatment of both dye layers and NC films, the NC surface chemistry, the dye concentration, and the solution solvent from which the dyes are deposited were found to affect the performance of photochemical sensitization processes.

Acknowledgment. This work was partially supported by Progetto MIUR D. M. n.1105 (9 October 2002) funding program. INSTM (Italy) is also gratefully acknowledged. We also thank Mr. Sergio Nuzzo and Mr. Giovanni Lasorella for their technical support.

References and Notes

(1) Nelson, J. *Curr. Opin. Solid State Mater. Sci.* **2002**, *6*, 87.
(2) Arici, E.; Sariciftci, N. S.; Meissner, D. In *Encyclopedia of Nanoscience and Nanotechnology*; Nalwa, H. S., Ed.; American Scientific: Los Angeles, CA, 2004; p 1.
(3) Grätzel, M. *J. Photochem. Photobiol. A: Chem.* **2004**, *164*, 3.
(4) Beek, W. J. E.; Wienk, M. M.; Janssen, R. A. J. *Adv. Mater.* **2004**, *16*, 1009.
(5) Hagfeldt, A.; Grätzel, M. *Chem. Rev.* **1995**, *95*, 49.
(6) Whorle, D.; Kreienhoop, L.; Schlettwein, D. In *Phthalocyanines, Properties and Applications*; Leznoff, C. C., Lever, A. B. P., Eds.; VCH: Weinheim, Germany, 1996; Vol. 4, p 1.
(7) Salafsky, J. *Phys. Rev. B* **1999**, *59*, 10885.
(8) Greenham, N. C.; Peng, X.; Alivisatos, A. P. *Phys. Rev. B* **1996**, *54*, 17628.
(9) Tracey S. M.; Hodgson, S. N. B.; Ray, A. K. *J. Sol Gel Sci. Technol.* **1998**, *13*, 219.
(10) Hagfeldt, A.; Schlichthörl, G.; Nozik, A. J.; Grätzel, M.; Frank, A. J. *J. Phys. Chem. B* **1997**, *101*, 2576.
(11) Hadgson, S.; Wilkie, J. *Int. Ceram.* **2001**, *1*, 49.
(12) Petrella, A.; Tamborra, M.; Curri, M. L.; Cosma, P.; Striccoli, M.; Cozzoli, P. D.; Agostiano, A. *J. Phys. Chem. B* **2005**, *109*, 1554.
(13) Ingrosso, C.; Petrella, A.; Curri, M. L.; Striccoli, M.; Cosma, P.; Cozzoli, P. D.; Agostiano, A. *Appl. Surf. Sci.* **2005**, *246*, 367.

(14) Ingrosso, C.; Petrella, A.; Curri, M. L.; Striccoli, M.; Cosma, P.; Cozzoli, P. D.; Agostiano, A. *Electrochim. Acta* **2006**, *51*, 5120.
(15) Alivisatos, A. P. *J. Phys. Chem.* **1996**, *100*, 13226.
(16) Alivisatos, A. P. *Science* **1996**, *271*, 933.
(17) Grem, G.; Leitzky, G.; Ullrich, B.; Leising, G. *Adv. Mater.* **1992**, *4*, 36.
(18) Greenham, N. C.; Moratti, S. C.; Bradley, D. D.; Friend, R.; Holmes, A. B. *Nature (London)* **1993**, *365*, 628.
(19) Dittmer, J. J.; Marseglia, E. A.; Friend, R. H. *Adv. Mater.* **2000**, *12*, 1270.
(20) Pollard, J. A.; Zhang, D.; Downing, J. A.; Knorr, F. J.; McHale, J. L. *J. Phys. Chem. A* **2005**, *109*, 11443.
(21) Tennakone, K.; Kottegoda, I. R. M.; De Silva, L. A. A.; Perera, V. P. S. *Semicond. Sci. Technol.* **1999**, *14*, 975.
(22) Bandaranayake, P. K. M.; Jayaweera, P. V. V.; Tennakone, K. *Sol. Energy Mater. Sol. Cells* **2003**, *76*, 57.
(23) Tennakone, K.; Bandara, J.; Bandaranayake, P. K. M.; Kumara, G. R. A.; Konno, A. *Jpn. J. Appl. Phys.* **2001**, *40*, L732.
(24) Reutergardh, L. B.; Iangphasuk, M. *Chemosphere* **1999**, *35*, 585.
(25) Grätzel, M. In *Semiconductor Nanoclusters—Physical, Chemical, and Catalytic Aspects*; Kamat, P. V., Meisel, D., Eds.; Elsevier Science B.V.: Amsterdam, 1997; p 417.
(26) Wróbel, D.; Boguta, A. *J. Photochem. Photobiol. A: Chem.* **2002**, *150*, 67.
(27) Qu, S.; Gao, Y.; Zhao, C.; Wang, Y.; Fu, S.; Song, Y.; Wang, D.; Qiu, J.; Zhu, C. *Chem. Phys. Lett.* **2003**, *367*, 767.
(28) Choi, M. T. M.; Li, P. P. S., Ng, D. K. P. *Tetrahedron* **2000**, *56*, 3881.
(29) Wróbel, D.; Goc, J.; Ion, R. M. *J. Mol. Struct.* **1998**, *450*, 239.
(30) Wróbel, D.; Boguta, A.; Ion, R. M. *J. Mol. Struct.* **2001**, *595*, 127.
(31) Ferraudi, G. In *Phthalocyanines, Properties and Applications*; Leznoff C. C., Lever A. B. P., Eds.; VCH: New York, 1989; Vol. 1, p 291.
(32) Sharman, W. H.; Allen, S. M.; van Lier, J. E. *Methods Enzymol.* **2000**, *319*, 375.
(33) Rao, D. V. G. L. N.; Aranda, F. J.; Roach, J. F.; Remy, D. E. *Appl. Phys. Letter* **1991**, *58*, 1241.
(34) Nordwood, R. A.; Sounik, J. R. *Appl. Phys. Lett.* **1992**, *60*, 295.
(35) Saito, T.; Iwakabe, Y., Kobayashi, T.; Suzuki, S.; Iwayanagi, T. *J. Phys. Chem.* **1994**, *98*, 2726.
(36) Mizuguchi, J.; Rihs, G.; Karfunkel, H. R. *J. Phys. Chem.* **1995**, *99*, 16217.
(37) Fujii, A.; Yoshida, M.; Ohmori, Y.; Yoshino, K. *Jpn. J. Appl. Phys.* **1996**, *35*, L37.
(38) Namba, N. In *Phthalocyanine—Chemistry and Functions*; Shirai, Y., Kobayashi, N., Eds.; IPC: Tokyo, 1997; p 247.
(39) Ray, A. K.; Tracey, S. M.; Hodgson, S. N. B. *J. Phys. D: Appl. Phys.* **2003**, *36*, 1409.
(40) Blasse, G.; Dirksen, G. J.; Meijerink, A.; van der Pol, J. F.; Neeleman, E.; Drenth, W. *Chem. Phys. Lett.* **1989**, *154*, 420.
(41) Popovic, Z. D.; Menzel, E. R. *J. Chem. Phys.* **1979**, *71*, 5090.
(42) Zelina, J. P.; Njue, C. K.; Rusling, J. F.; Kamau, G. N.; Masila, M.; Kibugu, J. *J. Porphyrins Phthalocyanines* **1999**, *3*, 188.
(43) Siggel, U.; Bindig, U.; Endisch, C.; Komutsu, T.; Tsuchida, E.; Voigt, J.; Fuhrhop, J.-H. *Ber. Bunsen-Ges. Phys. Chem.* **1996**, *100*, 2070.
(44) Menger, F. M. *Proc. Natl. Acad. Sci.* **2002**, *99*, 4818.
(45) Ferren, C.; FitzGerald, S.; Beeby, A.; Bryce, M. *Chem. Commun.* **2002**, 572.
(46) Schelly, Z. A.; Harward, D. J.; Hemmes, P.; Eyrig, E. M. *J. Phys. Chem.* **1970**, *74*, 3040.
(47) Van Nostrum, C. F.; Picken, S. J.; Schouten, A.-J.; Nolte, R. J. M. *J. Am. Chem. Soc.* **1995**, *117*, 9957.
(48) Amaral, C. L. C.; Politi, M. J. *Langmuir* **1997**, *13*, 4219.
(49) Togashi, D. M.; Costa, S. M. B.; Sobral, A. J. F. N.; Gonsalves, A. M. d'A. R. *J. Phys. Chem. B* **2004**, *108*, 11344.
(50) Scheibe, G. *Angew. Chem.* **1936**, *138*, 1009.
(51) Scheibe, G. *Angew. Chem.* **1937**, *50*, 51.
(52) Jelly, E. E. *Nature* **1937**, *139*, 631.
(53) von Berlepsch, H.; Regenbrecht, M.; Dahne, S.; Kirstein, S.; Bottcher, C. *Langmuir* **2002**, *18*, 2901.
(54) Barber, D. C.; Freitag-Beeston, R. A.; Whitten, D. G. *J. Phys. Chem.* **1991**, *95*, 4074.
(55) Kobayashi, N. *J. Phorphyrins Phthalocyanines* **2000**, *4*, 377.
(56) Khazraji, A. C.; Hotchandani, S.; Das, S.; Kamat, P. V. *J. Phys. Chem. B* **1999**, *103*, 4693.
(57) Kalyanasundaram, K.; Grätzel, M. *Coord. Chem. Rev.* **1998**, *177*, 347.
(58) Curri, M. L.; Petrella, A.; Striccoli, M.; Cozzoli, P. D.; Cosma, P.; Agostiano, A. *Synth. Met.* **2003**, *139*, 593.
(59) Hanglein, A. *Chem. Rev.* **1989**, *89*, 1861.
(60) Amao, Y.; Komori, T. *Langmuir* **2003**, *19*, 8872.
(61) He, J.; Benkö, G.; Korodi, F.; Polivka, T.; Lomoth, R.; Akermark, B.; Sun, L.; Hagfeldt, A.; Sundström, V. *J. Am. Chem. Soc.* **2002**, *124*, 4922.
(62) Cozzoli, P. D.; Curri, M. L.; Agostiano, A.; Leo, G.; Lomascolo, M. *J. Phys. Chem. B* **2003**, *107*, 4756.
(63) Spanhel, L.; Anderson, M. A. *J. Am. Chem. Soc.* **1991**, *113*, 2826.
(64) Cozzoli, P. D.; Kornowski A.; Weller H. *J. Am. Chem. Soc.* **2003**, *125*, 14539.
(65) Wróbel, D.; Hanyz, I.; Bartkowiak, R.; Ion, R. M. *J. Fluoresc.* **1998**, *8*, 191.
(66) Kobayashi, N.; Togashi, M.; Osa, T.; Ishii, K.; Yamauchi, S.; Hino, H. *J. Am. Chem. Soc.* **1996**, *118*, 1073.
(67) Davidson, A. T. *J. Chem. Phys.* **1982**, *77*, 168.
(68) Wang, Y.; Chen, H.-Z.; Li, H. Y.; Wang, M. *Mater. Sci. Eng. B* **2005**, *117*, 296.
(69) Deng, H.; Lu, Z.; Mao, H.; Xu, H. *Chem. Phys.* **1997**, *221*, 323.
(70) Lu, X.; Hipps, K. W. *J. Am. Chem. Soc.* **1996**, *118*, 7197.
(71) Ding, H.; Wang, S.; Xi, S. *J. Mol. Struct.* **1999**, *475*, 175.
(72) Cory, M. G.; Hirose, H.; Zerner, M. C. *Inorg. Chem.* **1995**, *34*, 2969.
(73) Agostiano, A.; Della Monica, M.; Palazzo, G.; Trotta, M. *Biophys. Chem.* **1993**, *47*, 193.
(74) Lee, K.; Sabelli, N. H.; LeBreton, P. R. *J. Phys. Chem.* **1982**, *86*, 3926.
(75) Janczak, J.; Kubiak, R. *Polyhedron* **2001**, *20*, 2901.
(76) Slota, R.; Dyrda, G. *Inorg. Chem.* **2003**, *42*, 5743.
(77) Ogunsipe, T.; Nyokong, T. *J. Mol. Struct.* **2004**, *689*, 89.
(78) Gouterman, M. G. In *The Phorphyrins*; Dolphin, D., Ed.; Academic Press: New York, 1978; Vol. 3, p 1.
(79) Vincete, P. S.; Voigt, E. M.; Rieckhoff, K. E. *J. Chem. Phys.* **1971**, *55*, 4131.
(80) Micali, N.; Romeo, A.; Laceri, R.; Purrello, R.; Mallamace, F.; Monsu Scolaro L. *J. Phys. Chem. B* **2000**, 104, 9417.
(81) Pasternack, R. F.; Collings, P. J. *Science* **1995**, *269*, 935.
(82) Bedja, I.; Kamat, P. V.; Hua, X.; Lappin, A. G.; Hotchandani, S.; *Langmuir* **1997**, *13*, 2398.
(83) Drechsel, J.; Männig, B.; Gebeyehu, D.; Pfeiffer, M.; Leo, K.; Hoppe, H. *Org. Electron.* **2004**, 5, 175.
(84) Boudemjema, B.; Guillard, G.; Gamoudi, M.; Maitrot, M.; André, J. J.; Martin, M.; Simon, J. *J. Appl. Phys.* **1984**, 56, 2323.
(85) Nuesch, F.; Carrara, M.; Schaer, M.; Romero, D. B.; Zuppiroli, L. *Chem. Phys. Lett.* **2001**, *347*, 311.
(86) Shihub, S. H.; Gould, R. D. *Thin Solid Films* **1996**, *390*, 290.
(87) Sakohara, S.; Tickanen, L. D.; Anderson, M. A. *J. Phys. Chem.* **1992**, *96*, 11086.
(88) Huynh, W. U.; Dittmer, J.; Alivisatos, A. P. *Science* **2002**, *295*, 2425.
(89) Bakueva, L.; Masikkin, S.; Hines, M. A.; Chang, T. W. F.; Tzolov, M.; Scholes, G. D.; Sargent, E. H. *Appl. Phys. Lett.* **2003**, *82*, 2895.